balance between the field energy and the energy difference between the normal and superconducting phases. This condition implies that the field strength inside the vortex is always equal to the critical field, and $r_c^2 \sim \nu \lambda_L \xi_0$, where λ_L is the London penetration depth ($\lambda_L^{-2} = 4\pi n e^2/\mu c^2$). We have here neglected surface effects which may be significant for small ν. Such vortex lines cannot be produced by the usual method by which the flux is trapped in a multiply connected domain, since the external field required to lower these states below the field-free state is equal to or greater than the critical field. A method for producing these states would be to first trap the flux in a multiply connected domain, in which the core is filled with another metal with a lower critical temperature. A further lowering of the temperature will thus make the sample simply connected and the trapped flux is expected to go into one or a number of vortex lines.[12]

ACKNOWLEDGMENT

We would like to acknowledge stimulating discussions with Professors Niels Bohr and H. Højgård Jensen.

[12] *Note added in proof.* Observations of trapped flux in simply connected superconductors have been made in connection with studies of intermediate state phenomena [see, e.g., D. M. Balashova and D. V. Sharvin, Soviet Physics—JETP **4**, 54 (1957); A. L. Schawlow and G. E. Devlin, Phys. Rev. **110**, 1011 (1958); W. de Sorbe and W. A. Healy, G. E. Report No. 61-RL-274314, July, 1961.] We are indebted to Dr. Morits, Dr. Nielsen, and Dr. Radhakrishna for calling these experiments to our attention and for interesting discussions of their significance in relation to the above considerations.

PHYSICAL REVIEW VOLUME 125, NUMBER 2 JANUARY 15, 1962

Interband Transitions for Metals in a Magnetic Field

M. S. DRESSELHAUS AND G. DRESSELHAUS
Lincoln Laboratory, Massachusetts Institute of Technology, Lexington, Massachusetts*
(Received August 30, 1961)

A quantum-mechanical derivation of the frequency and magnetic field dependence of the optical reflection and transmission in metals is given. Both interband and intraband direct transitions are considered and explicit results are obtained for a model of two simple parabolic bands having energy extrema at $\mathbf{k}=0$. Spin splitting is neglected. The calculated line shape is in good agreement with the magnetoreflection experiment of Brown *et al.* in bismuth. The results for the limiting cases of zero interband coupling or of zero magnetic field are in agreement with previous work. The study of the interband transitions in a magnetic field is shown to yield valuable information on the band structure of metals. The advantage of this method over magnetoplasma and zero-field interband studies is discussed.

I. INTRODUCTION

THE study of electronic transitions between the valence and conduction bands has yielded valuable information on the energy band structure of semiconductors.[1–5] It is of interest to ask whether similar studies can provide information on the band structure of metals.

There are two basic differences between a metal and a semiconductor, which affect the optical properties. Since, in a metal there are occupied states in the conduction band, the interband transitions are dependent on the position of the Fermi energy in the conduction band. Furthermore, the ordinary conduction processes of the "free carriers" in a good metal give rise to a background absorption, which is generally much larger than the interband effects.

This study was motivated by the observation of a resonant phenomenon in the reflection of infrared radiation from the surface of a single crystal of bismuth as the magnetic field was increased.[6] This resonant phenomenon was associated with transitions from Landau levels in the valence band to Landau levels in the conduction band. The data on Bi were analyzed by analogy with the work on the semiconductors[7,8] to yield values of the energy gap, and the effective mass and spectroscopic splitting factor for the conduction and valence bands. This calculation lends support to the method of analysis used in the interpretation of the bismuth data.

The object of this investigation is to determine the frequency and magnetic field dependence of the power reflection and transmission in metals. Particular emphasis is given to the effect of the magnetic field on the interband transitions and on the free-carrier

* Operated with support from the U. S. Army, Navy, and Air Force.

[1] L. H. Hall, J. Bardeen, and F. J. Blatt, Phys. Rev. **95**, 559 (1954).
[2] W. C. Dash and R. Newman, Phys. Rev. **99**, 1151 (1955).
[3] G. G. Macfarlane and V. Roberts, Phys. Rev. **97**, 1714 (1955); **98**, 1865 (1955).
[4] R. J. Elliott, T. P. Mclean, and G. G. Macfarlane, Proc. Phys. Soc. (London) **72**, 553 (1958).
[5] M. Okazaki, Progr. Theoret. Phys. (Kyoto) **25**, 163 (1961).
[6] R. N. Brown, J. G. Mavroides, M. S. Dresselhaus, and B. Lax, Phys. Rev. Letters **5**, 243 (1960).
[7] E. Burstein, G. S. Picus, H. A. Gebbie, and F. Blatt, Phys. Rev. **103**, 826(L) (1956).
[8] S. Zwerdling, B. Lax, L. M. Roth, and K. J. Button, Phys. Rev. **114**, 80 (1959); L. M. Roth, B. Lax, and S. Zwerdling, *ibid.* **114**, 90 (1959).

absorption. Power reflection and transmission curves are presented for both constant magnetic field as a function of frequency and constant frequency as a function of magnetic field. The orientation of the magnetic field parallel to the optical electric field and to the sample surface is chosen for simplicity.

II. THEORY

The power reflection R_H at a metal interface in a field H is determined by the surface impedance of the metal $Z_H(0)$,[9]

$$R_H=\left|\frac{Z_H(0)-4\pi/c}{Z_H(0)+4\pi/c}\right|^2, \tag{1}$$

in which $4\pi/c$ is the impedance of free space. The power T_H transmitted through a thickness δ of sample depends on R_H and on the spatial variation of the rf electric and magnetic fields in the metal. The special case of an exponential decay of the rf electric field inside the metal,

$$E(z)=E(0)e^{i(K_1+iK_2)z}, \tag{2}$$

in which z is the distance into the metal, is characteristic of the classical skin effect and of the slightly anomalous metal. Since Eq. (2) is generally valid at optical frequencies, the power transmission through a thickness δ of sample can be written as

$$T_H=\frac{(1-R_H)^2\exp(-2K_2\delta)}{1-R_H^2\exp(-4K_2\delta)}. \tag{3}$$

The surface impedance and spatial dependence of the rf fields are found from solution of the Maxwell Equations, using suitable constitutive equations to relate the current to the fields and the polarization to the fields.

The surface of the sample is considered to be flat and is taken as the xy plane with the z direction normal to the surface and extending into the metal. The rf electric field is taken along the x direction and has spatial variation $E_x(z)$. The static magnetic field is also taken along the x direction. The Hall fields may be coupled into the problem either along the y or z directions. For simplicity, specular reflection boundary conditions are used for the electron trajectory.[10] Then the semi-infinite metal can be replaced by an equivalent infinite medium with current sheets at $z=0$ given by the rf current density $\mathbf{j}_{b,\mathrm{rf}}$,

$$\mathbf{j}_{b,\mathrm{rf}}=-\frac{c}{2\pi}[\mathbf{H}_{\mathrm{rf}}(0)\times\hat{\mathbf{k}}]\delta(z), \tag{4}$$

and by the dc current density $\mathbf{j}_{b,\mathrm{dc}}$,

$$\mathbf{j}_{b,\mathrm{dc}}=(c/2\pi)H\delta(z)\hat{\mathbf{j}}, \tag{5}$$

in which $\hat{\mathbf{j}}$ and $\hat{\mathbf{k}}$ are unit vectors in the y and z directions, respectively.

To calculate the surface impedance it is convenient to write the Fourier transform of Maxwell's equations for the rf fields,

$$\left(\kappa_z^2-\frac{\omega^2}{c^2}\right)E_\alpha(\kappa_z)-\frac{4\pi\omega^2}{c^2}P_\alpha(\kappa_z)+\frac{4\pi i\omega}{c^2}j_\alpha(\kappa_z)+\frac{2}{(2\pi)^{\frac{1}{2}}}E_x'(0)=0, \tag{6}$$

$$E_z(\kappa_z)+4\pi P_z(\kappa_z)-\frac{4\pi i}{\omega}j_z(\kappa_z)=0, \tag{7}$$

in which $\mathbf{P}$ is the polarization vector,

$$E_\alpha'(0)=(\partial E_\alpha/\partial z)_{z=0},\quad \alpha=x,\ y,$$

and the normalization for the Fourier transform is

$$E_\alpha(\kappa_z)=\frac{1}{(2\pi)^{\frac{1}{2}}}\int_{-\infty}^{\infty}e^{i\kappa_z z}E_\alpha(z)dz. \tag{8}$$

The surface impedance can be found once the constitutive equations relating $\mathbf{j}$ and $\mathbf{E}$, and $\mathbf{P}$ and $\mathbf{E}$ are known. It can be shown that a self-consistent field calculation of the complex conductivity contains the screening or polarization effects associated with the real part of the complex dielectric constant. Thus, a self-consistent field calculation of the current-field relation is sufficient to determine the optical properties.

Since the interband transitions between Landau levels are a quantum-mechanical phenomena, a quantum-mechanical calculation of the current-field relation is necessary. The density matrix technique is used here to solve the steady-state problem. The periodicity of the lattice is taken into account and the electron collisions are handled through a relaxation time. Different relaxation times are introduced for scattering processes involving a single band and those involving interband transitions.

The Hamiltonian for the system is

$$\mathcal{H}=\mathcal{H}_0+\mathcal{H}_1, \tag{9}$$

in which the unperturbed Hamiltonian is taken as

$$\mathcal{H}_0=\frac{[\mathbf{p}-(e/c)\mathbf{A}_0]^2}{2m_0}+V_P(\mathbf{r}), \tag{10}$$

m_0 being the free electron mass, and $V_P(\mathbf{r})$ the periodic potential of the metal lattice. The gauge for the vector potential $\mathbf{A}_0$ for the static magnetic field H is for convenience chosen as

$$\mathbf{A}_0=yH\hat{\mathbf{k}}. \tag{11}$$

[9] R. B. Dingle, Physica 22, 683 (1956).

[10] The results for the power reflection and transmission are independent of boundary conditions for a local current-field relation and are rather insensitive to boundary conditions when nonlocal terms are included.

The time-dependent perturbation $\mathcal{H}_1$ arising from the rf fields is considered only for terms linear in the fields,

$$\mathcal{H}_1 = -\frac{e}{2m_0 c}(\mathbf{p}\cdot\mathbf{A}+\mathbf{A}\cdot\mathbf{p}), \tag{12}$$

$\mathbf{A}$ being the vector potential for the rf fields,

$$\mathbf{A} = -\frac{\hat{\mathbf{i}}c}{\omega}E_x(z)\sin\omega t, \tag{13}$$

in which $\hat{\mathbf{i}}$ is a unit vector in the x direction. The solution of the unperturbed Schrödinger equation for the magnetic field problem,

$$\mathcal{H}_0\Psi_{n,\mathbf{q}}{}^{l} = \mathcal{E}_n{}^{l}(\mathbf{q})\Psi_{n,\mathbf{q}}{}^{l}, \tag{14}$$

in the effective-mass approximation is[11]

$$\Psi_{n,\mathbf{q}}{}^{l}(\mathbf{r}) = (2\pi)^{\frac{1}{2}}e^{i(q_x x+q_z z)}\phi_l(y-\lambda^2 q_z)u_{n0}(\mathbf{r}), \tag{15}$$

and is periodic in x and z.

The choice of gauge for the dc field given in Eq. (11) results in harmonic oscillator motion in the y direction described by the harmonic oscillator function $\phi_l(y)$ and modified plane wave behavior in the x and z directions, involving the two dimensional wave vector $\mathbf{q}=q_x\hat{\mathbf{i}}+q_z\hat{\mathbf{k}}$, and the Bloch function at $\mathbf{k}=0$, $u_{n0}(\mathbf{r})$. For simplicity all band extrema are taken at $\mathbf{k}=0$. The harmonic oscillator wave functions are displaced by the distance $\lambda^2 q_z$, in which the characteristic length λ is given by

$$\lambda^2 = \hbar/m_n{}^{*}\omega_c{}^{(n)} = c\hbar/eH, \tag{16}$$

and is independent of band parameters. The parameters $m_n{}^{*}$ and $\hbar\omega_c{}^{(n)}$ are, respectively, the effective mass in the nth band and the spacing of the harmonic oscillator or Landau levels in the nth band,

$$\hbar\omega_c{}^{(n)} = e\hbar H/m_n{}^{*}c. \tag{17}$$

The quantum numbers n and l denote, respectively, the band index and the harmonic oscillator state. The normalization of the unperturbed wave functions is taken as

$$\int \Psi_{n',\mathbf{q}'}{}^{l'*}(\mathbf{r})\Psi_{n,\mathbf{q}}{}^{l}(\mathbf{r})d\mathbf{r} = \delta_{n,n'}\delta_{l,l'}\delta(\mathbf{q}-\mathbf{q}'), \tag{18}$$

in which the integration is carried out throughout the volume of the crystal.

In the effective-mass approximation, the energy eigenvalues of Eq. (14) relative to the energy at the extremum of the nth band $\mathcal{E}_n(0)$ are

$$\mathcal{E}_n{}^{l}(\mathbf{q}) = \hbar^2 q_x{}^2/2m_n{}^{*}+\hbar\omega_c{}^{(n)}(l+\tfrac{1}{2})+\mathcal{E}_n(0). \tag{19}$$

The notation used for matrix elements of an operator $\mathcal{O}$ in the various representations is

$$(n,l,\mathbf{q}|\,\mathcal{O}\,|n',l',\mathbf{q}') = \int d\mathbf{r}\,\Psi_{n,\mathbf{q}}{}^{l*}(\mathbf{r})\mathcal{O}\Psi_{n',\mathbf{q}'}{}^{l'}(\mathbf{r}), \tag{20}$$

when taken between the unperturbed wave functions,

$$\langle n,0|\,\mathcal{O}\,|n',0\rangle = \int d\mathbf{r}\,u_{n0}{}^{*}(\mathbf{r})\mathcal{O}u_{n'0}(\mathbf{r}), \tag{21}$$

when taken between the periodic part of the Bloch functions at $\mathbf{k}=0$, and

$$\{l|\,\mathcal{O}\,|l'\} = \int dy\,\phi_l{}^{*}(y)\mathcal{O}\phi_{l'}(y), \tag{22}$$

when taken between two harmonic oscillator states.

The mean value for the current density $\langle\mathbf{j}(\mathbf{r})\rangle$ can be written in terms of the wave functions for the unperturbed problem by use of the average density matrix[12] for the system at a time t, $\bar{\rho}(t)$,

$$\langle\mathbf{j}(\mathbf{r})\rangle = \sum_{n,l,n',l'}\int\int d\mathbf{q}d\mathbf{q}'\,\bar{\rho}_{n,\mathbf{q}}{}^{l};{}_{n',\mathbf{q}'}{}^{l'}\mathbf{j}_{n',\mathbf{q}'}{}^{l';}{}_{n,\mathbf{q}}{}^{l}. \tag{23}$$

The current density operator in the unperturbed representation is

$$\mathbf{j}_{n',\mathbf{q}'}{}^{l';}{}_{n,\mathbf{q}}{}^{l} = \frac{e}{2m_0}\Big\{\Psi_{n',\mathbf{q}'}{}^{l'*}\Big(\mathbf{p}-\frac{e}{c}\mathbf{A}_T\Big)\Psi_{n,\mathbf{q}}{}^{l} - \Psi_{n,\mathbf{q}}{}^{l}\Big(\mathbf{p}+\frac{e}{c}\mathbf{A}_T\Big)\Psi_{n',\mathbf{q}'}{}^{l'*}\Big\}, \tag{24}$$

in which $\mathbf{A}_T$ is the total vector potential $\mathbf{A}_T=\mathbf{A}_0+\mathbf{A}$. The equation of motion for the average density matrix is[11]

$$\frac{\partial\bar{\rho}}{\partial t} = \frac{i}{\hbar}[\bar{\rho}(t),\mathcal{H}]-\frac{\bar{\rho}-\rho_0}{\tau}. \tag{25}$$

Not only $\bar{\rho}$, but also the instantaneous value of the density matrix directly after a collision ρ_0 is time dependent,

$$\rho_0 = [1+\exp(\mathcal{H}-\epsilon_F)/kT]^{-1}, \tag{26}$$

in which ϵ_F is the Fermi energy. In the representation of the unperturbed wave functions, ρ_0 is almost diagonal[13]:

$$(n,l,\mathbf{q}|\,\rho_0(\mathcal{H})\,|n',l',\mathbf{q}') = \delta_{n,n'}\delta_{l,l'}\delta(\mathbf{q}-\mathbf{q}')f_0[\mathcal{E}_n{}^{l}(\mathbf{q})] + \frac{e\sin\omega t}{m_0\omega}(n,l,\mathbf{q}|\,p_x E_x(z)\,|n',l',\mathbf{q}') \times\Big[\frac{f_0[\mathcal{E}_n{}^{l}(\mathbf{q})]-f_0[\mathcal{E}_{n'}{}^{l'}(\mathbf{q}')]}{\mathcal{E}_n{}^{l}(\mathbf{q})-\mathcal{E}_{n'}{}^{l'}(\mathbf{q}')}\Big]+\cdots, \tag{27}$$

[11] J. M. Luttinger and W. Kohn, Phys. Rev. **97**, 869 (1955).

[12] R. Karplus and J. Schwinger, Phys. Rev. **73**, 1020 (1948).

[13] P. N. Argyres, Westinghouse Laboratory Research Report 60-94760-2-R6, 1955 (unpublished) and Phys. Rev. **99**, 1641 (1955).

and the average density matrix is

$$(n,l,\mathbf{q}|\bar{\rho}|n',l',\mathbf{q}')=\delta_{n,n'}\delta_{l,l'}\delta(\mathbf{q}-\mathbf{q}')f_0[\mathcal{E}_n{}^l(\mathbf{q})]$$
$$+\frac{e}{2im_0\omega}(n,l,\mathbf{q}|p_xE_x(z)|n',l',\mathbf{q}')$$
$$\times\left[\frac{f_0[\mathcal{E}_n{}^l(\mathbf{q})]-f_0[\mathcal{E}_{n'}{}^{l'}(\mathbf{q}')]}{\mathcal{E}_n{}^l(\mathbf{q})-\mathcal{E}_{n'}{}^{l'}(\mathbf{q}')}\right]$$
$$\times\left[\frac{[\mathcal{E}_n{}^l(\mathbf{q})-\mathcal{E}_{n'}{}^{l'}(\mathbf{q}')-i\hbar/\tau_{nn'}]e^{i\omega t}}{\hbar(\omega-i/\tau_{nn'})+[\mathcal{E}_n{}^l(\mathbf{q})-\mathcal{E}_{n'}{}^{l'}(\mathbf{q}')]}\right.$$
$$\left.-\frac{[\mathcal{E}_n{}^l(\mathbf{q})-\mathcal{E}_{n'}{}^{l'}(\mathbf{q}')-i\hbar/\tau_{nn'}]e^{-i\omega t}}{-\hbar(\omega+i/\tau_{nn'})+[\mathcal{E}_n{}^l(\mathbf{q})-\mathcal{E}_{n'}{}^{l'}(\mathbf{q}')]}\right]+\cdots. \quad (28)$$

The leading term of Eqs. (28) and (29) represents the equilibrium distribution in the absence of the perturbation, $f_0[\mathcal{E}_n{}^l(\mathbf{q})]$ being the Fermi distribution for energy $\mathcal{E}_n{}^l(\mathbf{q})$. The subscripts on the relaxation time $\tau_{nn'}$ allow τ to vary with the band index n and to be different for intraband conduction processes as opposed to interband transitions. The mean value of the current density is obtained by substitution of Eqs. (24) and (28) into Eq. (23) and by insertion of a factor of 2 for the electron spin. It is convenient to deal with the Fourier transform of the current density

$$\langle\mathbf{j}(\boldsymbol{\kappa})\rangle=\left(\frac{1}{2\pi}\right)^{\frac{3}{2}}\int_{-\infty}^{\infty}e^{i\boldsymbol{\kappa}\cdot\mathbf{r}}\langle\mathbf{j}(\mathbf{r})\rangle d\mathbf{r}, \quad (29)$$

in evaluating Eq. (23). The matrix elements which enter into the evaluation of $\langle\mathbf{j}(\boldsymbol{\kappa})\rangle$ are

$$(n,l,\mathbf{q}|e^{i\boldsymbol{\kappa}\cdot\mathbf{r}}|n',l',\mathbf{q}')$$
$$=\delta_{n,n'}\delta(q_x'-q_x+\kappa_x)\delta(q_z'-q_z+\kappa_z)\exp(i\lambda^2\kappa_yq_z)$$
$$\times\int dy\, e^{i\kappa_y y}\phi_l^*(y)\phi_{l'}(y+\lambda^2\kappa_z), \quad (30)$$

$$-\frac{e}{c}(n',l',\mathbf{q}'|\mathbf{A}|n,l,\mathbf{q})$$
$$=\frac{-ie\hat{\mathbf{i}}}{2\omega(2\pi)^{\frac{3}{2}}}(e^{i\omega t}-e^{-i\omega t})\delta_{n,n'}\delta(q_x-q_x')E_x(q_z-q_z')$$
$$\times\int dy\,\phi_{l'}^*(y)\phi_l(y-\lambda^2[q_z-q_z']), \quad (31)$$

$$-(e/c)(n',l',\mathbf{q}'|\mathbf{A}_0|n,l,\mathbf{q})$$
$$=-(eH_0/c)\hat{\mathbf{k}}\delta_{n,n'}\delta(\mathbf{q}-\mathbf{q}')\{l'|y+\lambda^2q_z|l\}, \quad (32)$$

$$(n',l',\mathbf{q}'|p_x|n,l,\mathbf{q})=\delta_{l,l'}\delta(\mathbf{q}-\mathbf{q}')(n',l,\mathbf{q}|p_x|n,l,\mathbf{q}), \quad (33)$$

$$(n',l',\mathbf{q}'|p_y|n,l,\mathbf{q})$$
$$=\delta(\mathbf{q}-\mathbf{q}')[\delta_{l,l'}\langle n',0|p_y|n,0\rangle+\delta_{n,n'}\{l'|p_y|l\}], \quad (34)$$

and

$$(n',l',\mathbf{q}'|p_z|n,l,\mathbf{q})$$
$$=\delta_{ll'}\delta(\mathbf{q}-\mathbf{q}')[\delta_{n,n'}\hbar q_z+\langle n',0|p_z|n,0\rangle]. \quad (35)$$

From the form of the unperturbed wave function of Eq. (15), it follows that the matrix element of p_x is independent of the quantum numbers l and q_z, and obeys the relation

$$(n,l,\mathbf{q}_0|p_x|n,l,\mathbf{q}_0)=\frac{m_0}{\hbar}\left[\frac{\partial\mathcal{E}_n{}^l(\mathbf{q})}{\partial q_x}\right]_{\mathbf{q}_0}, \quad (36)$$

and the f sum rule

$$\frac{2}{m_0}\sum_{n'\neq n}\frac{|(n,l,\mathbf{q}_0|p_x|n',l,\mathbf{q}_0)|^2}{\mathcal{E}_{n'}{}^l(\mathbf{q}_0)-\mathcal{E}_n{}^l(\mathbf{q}_0)}=1-\frac{m_0}{\hbar^2}\left(\frac{\partial^2\mathcal{E}_n{}^l(\mathbf{q}_0)}{\partial q_x{}^2}\right). \quad (37)$$

The mean value of the Fourier transform of the current is thus found to be

$$\langle\mathbf{j}(\boldsymbol{\kappa})\rangle=\sigma_{xx}(\kappa_z)E_x(\kappa_z)\hat{\mathbf{i}}, \quad (38)$$

in which complex conductivity is[14]

$$\sigma_{xx}(\kappa_z)=\frac{e^2}{2\pi^2i\lambda^2}\sum_{n,l,l'}\frac{1}{m_n{}^*}\left[\frac{|J_{l,l'}(\lambda^2\kappa_z)|^2(\omega-i/\tau_{nn})}{(\omega-i/\tau_{nn})^2-[\omega_c{}^{(n)}(l-l')]^2}\right]$$
$$\times\int dq_x f_0[\mathcal{E}_n{}^l(q_x)]+\frac{e^2\hbar}{2\pi^2i\lambda^2m_0{}^2}\sum_{\substack{n,n',l,l'\\ n'\neq n}}|J_{l,l'}(\lambda^2\kappa_z)|^2$$
$$\times\int dq_x\frac{\{f_0[\mathcal{E}_n{}^l(q_x)]-f_0[\mathcal{E}_{n'}{}^{l'}(q_x)]\}}{\mathcal{E}_n{}^l(q_x)-\mathcal{E}_{n'}{}^{l'}(q_x)}$$
$$\times|(n,l,\mathbf{q}|p_x|n',l,\mathbf{q})|^2\left[\frac{\mathcal{E}_n{}^{l'}(q_x)-\mathcal{E}_n{}^l(q_x)}{\hbar\omega[\mathcal{E}_n{}^l(q_x)-\mathcal{E}_{n'}{}^l(q_x)]}\right.$$
$$\left.-\frac{1}{\hbar(\omega-i/\tau_{nn'})+\mathcal{E}_n{}^l(q_x)-\mathcal{E}_{n'}{}^{l'}(q_x)}\right]+\cdots, \quad (39)$$

and

$$J_{l,l'}(\lambda^2\kappa_z)=\int dy\,\phi_l^*(y)\phi_{l'}(y-\lambda^2\kappa_z). \quad (40)$$

The form of Eq. (39) distinguishes between contributions to the conductivity which involve a single band index (intraband conductivity, $\sigma_{xx}{}^{\text{intra}}$) and those which involve two band indices (interband conductivity, $\sigma_{xx}{}^{\text{inter}}$). The expression for the interband conductivity is the usual anomalous skin effect result,[15] except that the effective mass has replaced the free electron mass. This particular magnetic field orientation introduces no Hall fields if the crystal is assumed to have cubic symmetry.

An explicit evaluation is made here for a two-band model: a single conduction band and a single valence

[14] S. Nakajima, *Advances in Physics*, edited by N. F. Mott (Taylor and Francis, Ltd., London, 1955), Vol. 4, p. 363.
[15] D. C. Mattis and G. Dresselhaus, Phys. Rev. 111, 403 (1958).

band with extrema at $\mathbf{k}=0$. Thus, the lower lying bands are not treated in detail, nor are the higher empty bands. The contribution from the internal atomic bands to the conductivity is treated macroscopically as a core polarization contribution, which can be taken as approximately frequency independent over the frequency range of interest. This type of two-band model is a reasonable approximation to a real metal if the photon energy is small compared with the energy gaps between the conduction band and the next-higher unfilled band and between the valence band and the next-lower filled band. Thus Eq. (39) is written as

$$\sigma_{xx}(\kappa_z)=\sigma_{xx}{}^{\text{core}}+\sigma_{xx,c}{}^{\text{intra}}(\kappa_z)+\sigma_{xx,cv}{}^{\text{inter}}(\kappa_z), \quad (41)$$

in which the core contribution is essentially dispersive and is related to the core dielectric constant $\epsilon_{xx}{}^{\text{core}}$ by

$$\sigma_{xx}{}^{\text{core}}=(i\omega/4\pi)\epsilon_{xx}{}^{\text{core}}. \quad (42)$$

The intraband contribution is considered for only the conduction band; the interband contribution contains only transitions between the valence and conduction bands. For simplicity, a spherical Fermi surface is introduced and any dependence of the effective mass on wave vector is neglected. The κ_z dependence of the conductivity is contained in the term $|J_{l,l'}(\lambda^2\kappa_z)|^2$. Since the leading term of $|J_{l,l'}(\lambda^2\kappa_z)|^2$ at optical frequencies is $\delta_{l,l'}$, the result is a local relation between current and field. The effect on the optical properties of the nonlocal terms in Eq. (39) is considered elsewhere.[16]

Using these approximations, the contribution to the intraband conductivity from the conduction band at $T=0°\text{K}$ can be written as

$$\sigma_{xx,c}{}^{\text{intra}}=\sigma_0\left(\frac{m_0}{m_c{}^*}\right)\sum_{l=0}^{l_F}\frac{3}{2}\frac{(l_F-l)^{\frac{1}{2}}}{(\eta\beta\xi)^{\frac{3}{2}}}, \quad (43)$$

in which the conductivity σ_0 is given by

$$\sigma_0=Ne^2\tau_c/m_0(1+i\omega\tau_c), \quad (44)$$

and the concentration of conduction electrons is given by

$$N=[(\eta\beta)^{\frac{3}{2}}/3\pi^2](2m^*\epsilon_g/\hbar^2)^{\frac{3}{2}}. \quad (45)$$

The effective masses for the conduction and valence bands are denoted by $m_c{}^*$ and $m_v{}^*$, respectively, and are related to the reduced effective mass by

$$1/m^*=1/m_v{}^*+1/m_c{}^*, \quad (46)$$

and to the dimensionless effective-mass parameter

$$\eta=1+m_c{}^*/m_v{}^*=m_c{}^*/m^*, \quad (47)$$

which is 2 for equal effective masses in the valence and conduction bands. The dimensionless Fermi energy parameter β measures the Fermi energy ϵ_F above the energy gap ϵ_g between the valence and conduction bands:

$$\beta=(\epsilon_F-\epsilon_g)/\epsilon_g. \quad (48)$$

The quantity l_F is related to the Fermi energy and to the cyclotron frequency for the conduction electrons, $\omega_c{}^{(c)}=eH/m_c{}^*c$, by

$$l_F=[\epsilon_F-\epsilon_c(0)]/\hbar\omega_c{}^{(c)}-\tfrac{1}{2}, \quad (49)$$

$\epsilon_c(0)$ denoting the bottom of the conduction band (see Fig. 1). The dimensionless magnetic field parameter $1/\xi$ is given by

$$\xi=\epsilon_g/\hbar\omega_c, \quad (50)$$

in which the reduced cyclotron frequency ω_c is equal to $\eta\omega_c{}^{(c)}$.

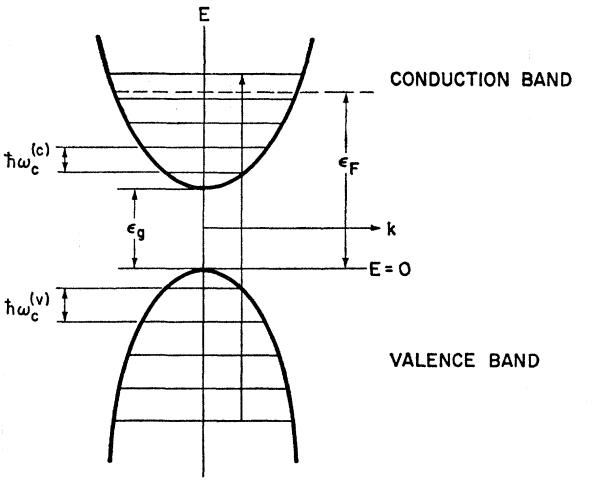

FIG. 1. The parabolic curves give the zero field $\mathcal{E}(\mathbf{k})$ vs $\mathbf{k}$ for the valence and conduction bands with extrema at $\mathbf{k}=0$. The Landau levels in the two bands are indicated.

The contribution to the interband conductivity from interband transitions between the valence and conduction bands is found by expanding the matrix element of p_x between these two bands $(v,l,\mathbf{q}|p_x|c,l,\mathbf{q})$ in a power series in q_x. The leading term represents the allowed transitions and is

$$\sigma_{xx,cv}{}^{\text{inter}}=3\sigma_0\frac{(\mu-i\alpha_c)}{(\mu-i\alpha_{cv})}\mathcal{C}_H\mathcal{G}(\xi,\mu;\alpha_{cv},\beta,\gamma,\eta), \quad (51)$$

in which the frequency- and magnetic-field-dependent function $\mathcal{G}(\xi,\mu;\alpha_{cv},\beta,\gamma,\eta)$ is given by

$$\mathcal{G}(\xi,\mu;\alpha_{cv},\beta,\gamma,\eta)=\tfrac{1}{2}\xi^{-\frac{1}{2}}(\eta\beta)^{-\frac{3}{2}}[2\mathcal{S}(1)-\mathcal{S}(1+\mu-i\alpha_{cv})-\mathcal{S}(1-\mu+i\alpha_{cv})], \quad (52)$$

and

$$\mathcal{S}(x)=\left[\sum_{l=0}^{l_{\max}}\frac{\tan^{-1}\{[(l_{\max}-l)/(l+\frac{1}{2}+\xi x)]^{\frac{1}{2}}\}}{(l+\frac{1}{2}+\xi x)^{\frac{1}{2}}}-\sum_{l=0}^{l_F}\frac{\tan^{-1}\{[(l_F-l)/(l+\frac{1}{2}+\xi x)]^{\frac{1}{2}}\}}{(l+\frac{1}{2}+\xi x)^{\frac{1}{2}}}\right]. \quad (53)$$

[16] M. S. Dresselhaus and G. Dresselhaus, Massachusetts Institute of Technology Lincoln Laboratory G-Report, 82G-0030 (unpublished), which is available at the M.I.T. Hayden Library.

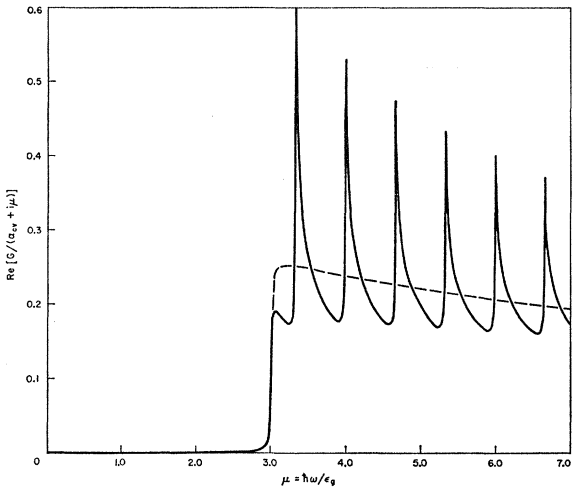

FIG. 2. Dimensionless plot of the frequency dependence of the real part of the interband conductivity for a high magnetic field $\xi=1.5$ (solid) and for zero magnetic field $\xi=\infty$ (dashed). The parameters are taken as $\alpha_{cv}=0.01$, $\beta=1.0$, $\gamma=20.0$, and $\eta=2.0$. (See text.)

A measure of the strength of the interband coupling characterizing each metal is

$$\mathcal{C}_H=|(v,0,0|p_x|c,0,0)|^2/m_0\epsilon_g, \tag{54}$$

and the quantities μ, α_{cv}, α_c, γ denote, respectively, the dimensionless frequency parameter

$$\mu=\hbar\omega/\epsilon_g, \tag{55}$$

the dimensionless interband relaxation parameter

$$\alpha_{cv}=\hbar/\tau_{cv}\epsilon_g, \tag{56}$$

the dimensionless conduction band relaxation parameter

$$\alpha_c=\hbar/\tau_c\epsilon_g, \tag{57}$$

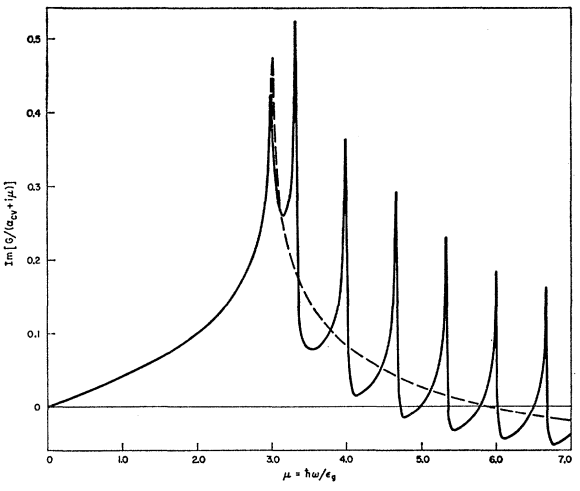

FIG. 3. Dimensionless plot of the frequency dependence of the imaginary part of the interband conductivity for a high magnetic field $\xi=1.5$ (solid) and for zero magnetic field $\xi=\infty$ (dashed). The parameters are taken as $\alpha_{cv}=0.01$, $\beta=1.0$, $\gamma=20.0$, and $\eta=2.0$. (See text.)

and the dimensionless band cutoff parameter

$$\gamma=(\epsilon_{\max}-\epsilon_g)/\epsilon_g. \tag{58}$$

The quantity $l_{\max}$ is related to the cutoff energy $\epsilon_{\max}$ by

$$l_{\max}=[\epsilon_{\max}-\epsilon_c(0)]/\hbar\omega_c^{(c)}-\tfrac{1}{2}. \tag{59}$$

The frequency and field dependence of the real and imaginary parts of $\sigma_{xx,cv}{}^{\text{inter}}$ are presented in Figs. 2, 3, 4, and 5 as dimensionless plots of the real and imaginary parts of $[\mathcal{G}/(\alpha_{cv}+i\mu)]$ vs μ and ξ with the values of the parameters taken as $\alpha_{cv}=0.01$, $\beta=1.0$, $\gamma=20$, and $\eta=2$. The discussion relevant to these curves is given in Sec. III.

The rf field dependence is thus found from Eqs. (6) and (41) to be

$$\frac{E_x(z)}{E_x'(0)}=-\frac{1}{\pi}\int_{-\infty}^{\infty}\frac{e^{-i\kappa_z z}d\kappa_z}{\kappa_z{}^2+(4\pi i\omega/c^2)\sigma_{xx}(\kappa_z)}=-\frac{e^{-Kz}}{K}, \tag{60}$$

in which K is related to the index of refraction n_H and the extinction coefficient k_H by[17]

$$K=(i\omega/c)(n_H-ik_H), \tag{61}$$

where $\mathrm{Re}(K)>0$ and

$$(n_H-ik_H)=(\epsilon_{xx}{}^{\text{core}})^{\frac{1}{2}}\left\{1-\frac{\mu_p{}^2}{\mu(\mu-i\alpha_c)}\left[\sum_{l=0}^{l_F}\frac{3}{2}\frac{(l_F-l)^{\frac{1}{2}}}{(\eta\beta\xi)^{\frac{3}{2}}}+C_H\left(\frac{\mu-i\alpha_c}{\mu-i\alpha_{cv}}\right)\mathcal{G}(\xi,\mu;\alpha_{cv},\beta,\gamma,\eta)\right]\right\}^{\frac{1}{2}}. \tag{62}$$

The relative importance of the "free-carrier absorption" in the conduction band and of the interband transitions as compared with the core dielectric constant is contained in the reduced plasma frequency parameter μ_p,

$$\mu_p{}^2=4\pi Ne^2\hbar^2/\epsilon_{xx}{}^{\text{core}}m_c{}^*\epsilon_g{}^2=b\beta^{\frac{3}{2}}/\epsilon_{xx}{}^{\text{core}}, \tag{63}$$

and in the effective coupling parameter C_H,

$$C_H=3\mathcal{C}_H(m_c{}^*/m_0). \tag{64}$$

From Eqs. (3) and (60), it follows that the power reflected at a metal interface in a field H is

$$R_H=\frac{(n_H-1)^2+k_H{}^2}{(n_H+1)^2+k_H{}^2}, \tag{65}$$

and the power transmitted through a thickness δ of sample is given by Eq. (3) with

$$K_2=\epsilon_0\mu k_H/\hbar c, \quad K_2>0. \tag{66}$$

Plots of the frequency and field dependence of R_H and T_H are presented in Figs. 6, 7, 8, and 9 for $\alpha_{cv}=0.01=\alpha_c$, $\beta=1.0$, $\gamma=20$, $\eta=2.0$, $C_H=1.5$, $b=2.5$, and $\epsilon_{xx}{}^{\text{core}}=9.0$.

[17] F. Seitz, *Modern Theory of Solids* (McGraw-Hill Book Company, Inc., New York, 1940), p. 632.

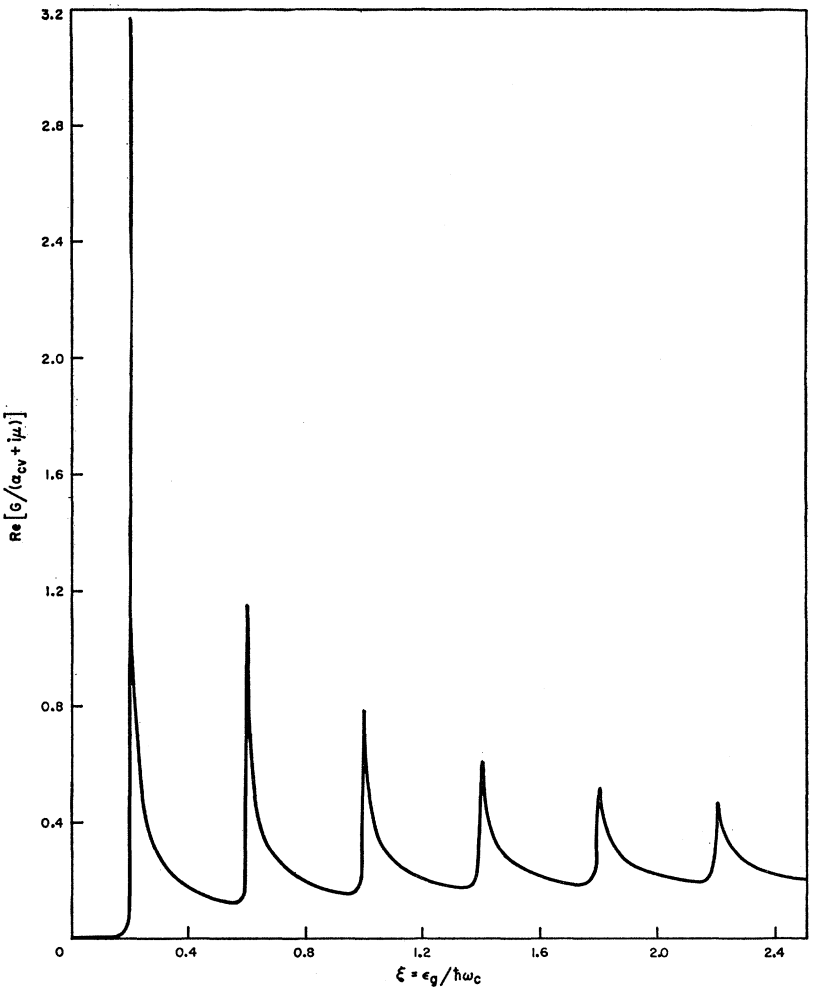

FIG. 4. Dimensionless plot of the real part of the interband conductivity vs $(1/H)$ for a photon energy $\mu=\hbar\omega/\epsilon_g=3.5$. The parameters are taken as $\alpha_{cv}=0.01$, $\beta=1.0$, $\gamma=20.0$, and $\eta=2.0$. (See text.)

The results for zero field ($\xi=\infty$) are also included. In this case, the frequency-dependent function $\mathcal{G}(\infty,\mu;\alpha_{cv},\beta,\gamma,\eta)$ reduces to

$$\mathcal{G}(\infty,\mu;\alpha_{cv},\beta,\gamma,\eta)=(\eta\beta)^{-\frac{3}{2}}[2S(1)-S(1+\mu-i\alpha_{cv})-S(1-\mu+i\alpha_{cv})], \quad (67)$$

with

$$S(x)=x^{\frac{1}{2}}[\tan^{-1}(\eta\beta/x)^{\frac{1}{2}}-\tan^{-1}(\eta\gamma/x)^{\frac{1}{2}}]. \quad (68)$$

The power reflection and transmission can be found from the limiting values of the index of refraction and of the extinction coefficient,

$$(n_0-ik_0)=(\epsilon_{xx}^{\text{core}})^{\frac{1}{2}}\left[1-\frac{\mu_p^2}{\mu(\mu-i\alpha_c)}\times\left\{1+C_0\left(\frac{\mu-i\alpha_c}{\mu-i\alpha_{cv}}\right)\mathcal{G}(\infty,\mu;\alpha_{cv},\beta,\gamma,\eta)\right\}\right]^{\frac{1}{2}}. \quad (69)$$

For simplicity, the field dependence of the parameters α_c, α_{cv}, β, η, C_H, b, and $\epsilon_{xx}^{\text{core}}$ is neglected in constructing the curves. The absolute magnitude of the transmission is fixed by choosing an energy gap of $\epsilon_g=1.0$ ev and a sample thickness of 0.5 micron.

III. DISCUSSION

In Figs. 2–9 it is seen that the direct transitions between the valence and conduction bands in a magnetic field result in a resonant and periodic variation of the real and imaginary parts of the interband conductivity and also of the observable quantities, the power reflection and power transmission. Information on the band structure of the metal is obtained from study of both the period of these resonances and of their line shape. In the absence of a magnetic field, the power reflection and transmission are affected by the interband transitions but not in a resonant manner.

Interband transitions in a magnetic field are energetically possible from a level l' in the valence band to a level l'' in the conduction band, where l'' denotes a Landau state above the Fermi energy, and l', a state in the valence band from which such a transition is

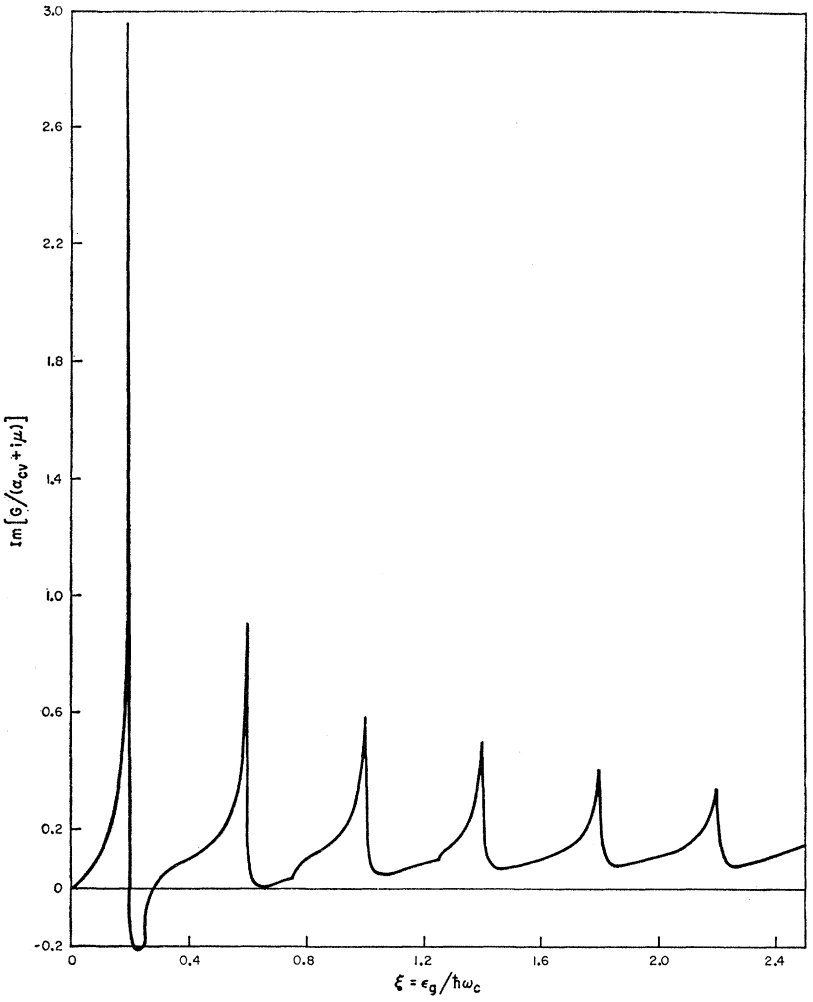

FIG. 5. Dimensionless plot of the imaginary part of the interband conductivity vs $(1/H)$ for a photon energy $\mu=\hbar\omega/\epsilon_g=3.5$. The parameters are taken as $\alpha_{cv}=0.01$, $\beta=1.0$, $\gamma=20.0$, and $\eta=2.0$. (See text.)

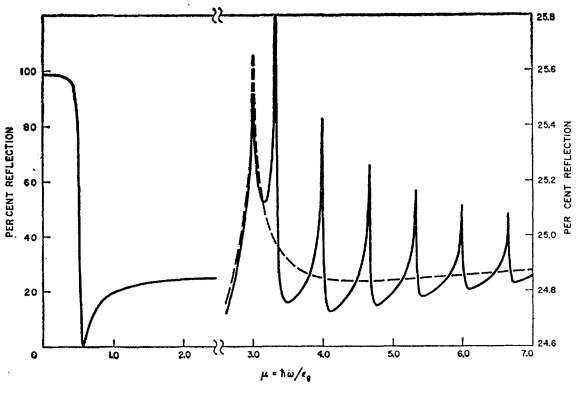

FIG. 6. Plot of the reflectivity vs the dimensionless frequency parameter μ for high magnetic field $\xi=1.5$ (solid) and for zero field $\xi=\infty$ (dashed). With the choice of parameters $\alpha_{cv}=0.01$, $\alpha_c=0.01$, $\beta=1.0$, $\gamma=20.0$, $\eta=2.0$, $C_H=1.5$, $b=2.5$, and $\epsilon_{xx}^{\text{core}}=9.0$, the low-frequency behavior features the free-carrier absorption. The interband transitions appear at higher frequencies as maxima in the reflectivity and are shown on an expanded scale.

allowed. Interband transitions between the two bands obey the selection rule $\Delta l=0$ if the high frequency current obeys a local current-field relation, if the two bands are simple quadratic bands, and if their energy extrema are located at the same point in $\mathbf{k}$ space.

The onset of the interband transitions in zero field is characterized by a sharp increase in the real part of the interband conductivity and by a cusp in the imaginary part as is seen in Figs. 2 and 3. In the presence of the magnetic field, additional peaks are seen in both the real and imaginary parts of $\sigma_{xx}^{\text{inter}}$ which correspond to the allowed transitions between the Landau levels. The magnitude and sharpness of these peaks increases as the relaxation time τ_{cv} increases (or α_{cv} decreases). This resonant behavior is observable either at constant magnetic field as a function of frequency (Figs. 2 and 3) or at constant frequency as a function of field (Figs. 4 and 5). On the basis of the simplified two-band model presented in this paper, these maxima as well as the maxima in the reflection and the minima in the transmission approximately

obey the condition

$$l+\tfrac{1}{2}+\xi(1-\mu)=0, \tag{70}$$

or $\hbar\omega=\epsilon_g+\hbar\omega_c(l+\frac{1}{2})$. This condition is exactly obeyed as the relaxation time becomes infinite. For a finite relaxation time, the reflection maxima are shifted to somewhat lower frequencies and higher fields, while the transmission minima occur at correspondingly higher frequencies and lower fields. The reflection maxima occur at the same field and frequency as the maxima of the imaginary part of the interband conductivity. The position of the transmission minima coincide with the maxima on the real part of the interband conductivity, which is associated with power loss. The intensity of the resonances increases with increasing field and with decreasing photon energy, provided that it is energetically possible to make a transition at all. Empirically, it is found that on reflection, the amplitude of the resonance maxima

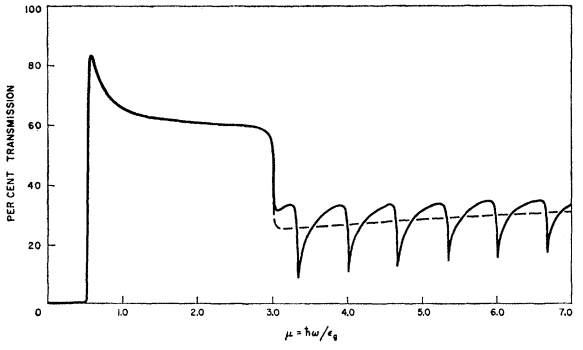

FIG. 7. Plot of the transmission vs the dimensionless frequency parameter μ for high magnetic field $\xi=1.5$ (solid) and for zero field $\xi=\infty$ (dashed). The parameters are the same as in Fig. 6. (See text.) At low frequencies the peak for the free-carrier absorption is seen. The interband transitions appear at higher frequencies as minima in the transmission.

increases linearly with field. The transmission minima in Fig. 9 are seen to approach essentially zero transmission for the lowest quantum number. Increasing quantum number not only decreases the magnitude of the resonances but also broadens them. The magnitude of the resonances increases with increasing (m_c^*/ϵ_g), but this ratio which determines b in Eq. (63) does not vary strongly from one material to another.

For the parameters chosen in Figs. 2–9, the departures of the reflection maxima and transmission minima from the resonant condition of Eq. (70) are about 0.2%. In reference 6, the resonant magnetic field was taken as the point on the resonance where the increase in the reflection was half the increase at the reflection maximum. For the values of the parameters chosen here, the departure of this point from the resonant condition of Eq. (70) is about 0.5% too low in magnetic field as compared with the reflection maximum which gives a value 0.2% too high in field. The lowest transition which ap-

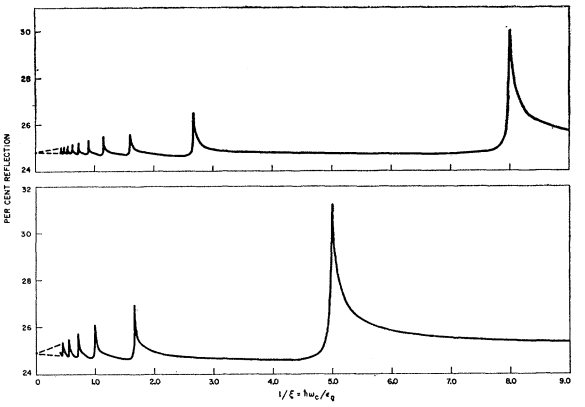

FIG. 8. Plot of the reflectivity vs the dimensionless field parameter $(1/\xi)=\hbar\omega_c/\epsilon_g$ at constant photon energy $\mu=3.5$ (lower curve) and $\mu=5.0$ (upper curve). The zero-field point is indicated. The parameters are the same as in Fig. 6. (See text.)

pears in the frequency plots of Figs. 2, 3, 6, and 7 is the $l=3$ transition, while the magnetic field plots of Figs. 4, 5, 8, and 9 include the $l=0$ and a few higher transitions. The resonances in Figs. 8 and 9 become so closely spaced as $H\rightarrow 0$ that only the zero-field point is shown and an envelope for the low-field behavior is indicated.

As the magnetic field increases a de Haas–van Alphen type of resonance is found both for the intraband conduction processes and for the interband transitions whenever a Landau level crosses the Fermi energy. This phenomena is of much smaller magnitude than the transitions between the Landau levels ($\approx 0.01\%$ as compared with several tenths of a percent) and is

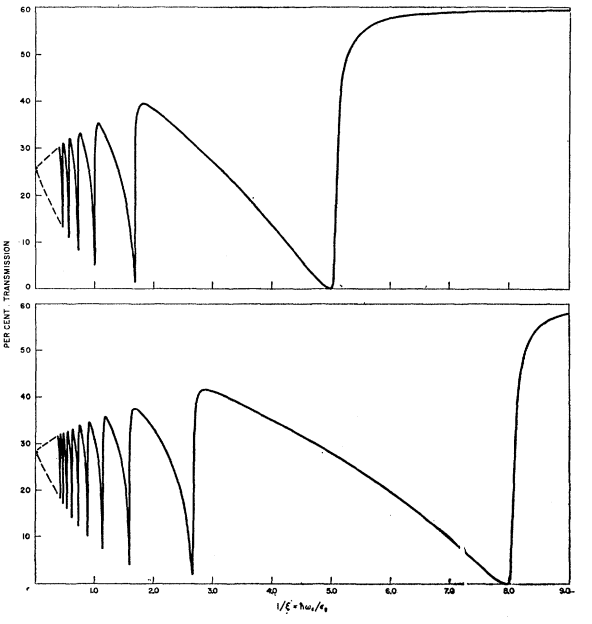

FIG. 9. Plot of the transmission vs the dimensionless field parameter $(1/\xi)=\hbar\omega_c/\epsilon_g$ at constant photon energy $\mu=3.5$ (lower curve) and $\mu=5.0$ (upper curve). The zero-field point is indicated. The parameters are the same as in Fig. 6. (See text.)

independent of photon energy. The imaginary part of the interband conductivity is sensitive to the de Haas–van Alphen effect and this effect can be seen on Fig. 5 at $\xi=0.25$, $\xi=0.75$, and $\xi=1.25$. The corresponding effect on the reflectivity at $1/\xi=4.0$, $1/\xi=1.33$, and $1/\xi=0.80$, is too small to be observed on the scale of Fig. 8. In constructing the figures, the variation of the Fermi energy (or β) with magnetic field which is associated with the de Haas-van Alphen effect has been neglected.

At photon energies lower than are energetically required for interband transitions, free carrier or plasma absorption is found and is observable either on reflection or on transmission as is seen in Figs. 6 and 7. If no interband transitions occur at any frequency at all, the photon energy characterizing the free-carrier absorption is $\mu_p\epsilon_g$. The presence of the interband transitions shifts the free-carrier absorption to either lower or higher frequencies. The magnitude of the shift increases with increasing proximity of the interband transitions to μ_p, with increasing interband coupling, and with increasing μ_p. Increasing the relaxation time sharpens the drop in the reflectivity and the rise in the transmission, but if α_c, $\alpha_{cv}\ll 1$, then α_c and α_{cv} are not as important in determining the exact frequency at which these edges occur. The presence of a magnetic field also shifts the plasma absorption edges. However, for this magnetic field orientation, the magnetic field effect is often of smaller magnitude than the shift produced by the interband transitions. On the scale used in Figs. 6 and 7 to present the free carrier absorption, the zero-field and high-field reflection and transmission curves are coincident.

The effect of the interband transitions on the free-carrier absorption has already been pointed out. Conversely, the free-carrier absorption influences the line shape of the interband transitions both in zero field and in the presence of a magnetic field. As μ_p increases, the magnitude of the resonances increases, but as μ_p approaches the onset of the interband transitions, the reflection and transmission curves show a confusion of free-carrier absorption and interband effects. The choice of the parameters taken here is reasonable for some metals and semimetals and has the virtue of separating the interband resonances from the free-carrier absorption. Some numerical examples are included here, but a more complete discussion is available elsewhere.[16] The reduced plasma frequency parameters $\mu_p^*(R)$ and $\mu_p^*(T)$ are chosen, respectively, as the point of inflection in the curves of the reflection and transmission vs frequency. With this criterion, the determination of $\mu_p^*(R)$ and $\mu_p^*(T)$ agree with each other to within 1%. The choice of the parameters $b=2.5$, $\beta=1.0$, and $\epsilon_{xx}^{\text{core}}=9.0$ results in $\mu_p=0.527$. If we take $\alpha_{cv}=\alpha_c=0.01$, $\gamma=20.0$, $\eta=2$, then $\mu_p^*(R)=0.525$ and $\mu_p^*(T)=0.530$ for $C_H=0$, $\xi=\infty$ (no magnetic field and no interband coupling); $\mu_p^*(R)=0.522$ and $\mu_p^*(T)=0.526$ for $C_H=1.5$, $\xi=\infty$ (no magnetic field and large interband coupling); $\mu_p^*(R)=0.530$ and $\mu_p^*(T)=0.534$ for $C_H=0$, $\xi=1.5$ (high magnetic field and no interband coupling); $\mu_p^*(R)=0.525$ and $\mu_p^*(T)=0.529$ for $C_H=1.5$, $\xi=1.5$ (high magnetic field and large interband coupling). Somewhat larger shifts in the plasma edge are observed for larger values of μ_p. The maximum value for C_H is found by assigning all the interband coupling from the f sum rule to the closest lying band.

The results of this work indicate that the study of the field variation of the free-carrier absorption is not as satisfactory a tool for the investigation of the band structure of metals as is the study of the interband transitions in a magnetic field. There are several reasons for this: (1) the magnitude of the field variation of $\mu_p^*(R)$ and $\mu_p^*(T)$ is comparable to the variation with other parameters, such as the interband coupling; (2) absolute values for the reflection and transmission are needed for the determination of $\mu_p^*(R)$ and $\mu_p^*(T)$; (3) the criterion for the determination of $\mu_p^*(R)$ and $\mu_p^*(T)$ is not clearly defined. These conclusions are relevant to $H_{\text{dc}}\|E_{\text{rf}}$ and different results are possible for $H_{\text{dc}}\pm E_{\text{rf}}$.

The study of the zero field transitions is also less satisfactory than the magnetic field experiment. There are also several reasons for this. (1) For the zero-field experiment, absolute values of the reflection and transmission vs photon energy are needed to locate the transitions. (2) Since interband effects on reflection are of the order of tenths of a percent to a few percent, a differential method is needed to increase the sensitivity. This is possible only in the magnetic field experiments. The interband effects are generally larger on transmission than on reflection, but the high attenuation of light by most metals imposes stringent requirements on the sample preparation both for zero-field and high-field measurements. (3) The magnetic field greatly simplifies the search for interband transitions, since the resonances can be observed over a wide range of frequency and field. (4) Not only is the magnetic field experiment more sensitive and convenient, but also more information is available. Both the spacing of the resonances and the line shape of a single resonance can be studied. The spacing of the resonances gives information on the effective masses of the valence and conduction bands and on the energy gap between them. The line shapes can give information on the magnitude of the interband coupling and the relaxation time for interband transitions.

ACKNOWLEDGMENTS

The authors have profited by stimulating conversations with Dr. B. Lax, Dr. J. G. Mavroides, and Dr. P. N. Argyres. We would like to thank Mrs. M. Clare Brown especially for carrying out the numerical computations.